NEW PLANAR AIR-BEARING MICROGRAVITY SIMULATOR FOR VERIFICATION OF SPACE ROBOTICS NUMERICAL SIMULATIONS AND CONTROL ALGORITHMS

Tomasz Rybus [(1)], Janusz Nicolau-Kukliński [(1)], Karol Seweryn [(1)], Tomasz Barciński [(2)], Monika Ciesielska [(1)], Kamil Grassmann [(1)], Jerzy Grygorczuk [(1)], Michał Karczewski [(1)], Marek Kowalski [(1)], Marcin Krzewski [(1)], Tomasz Kuciński [(1)], Jakub Lisowski [(1)], Rafał Przybyła [(1)], Konrad Skup [(1)], Tomasz Szewczyk [(1)], Roman Wawrzaszek [(1)]

[(1)] *Space Research Centre of the Polish Academy of Sciences, Bartycka 18a str., 00-716 Warsaw, Poland, trybus@cbk.waw.pl*

[(2)] *West Pomeranian University of Technology, Piastów 17 av., 70-310 Szczecin, Poland*

ABSTRACT

Control of a free-floating satellite-manipulator system is a challenging task, because motions of the robotic arm influence position and orientation of its base. On Earth it is difficult to perform tests of such system, as it lacks a fixed-base. One possible solution to perform these tests is based on application of planar air-bearings which provide negligible friction and allow free planar motion of the satellite-manipulator system on the granite table. This paper presents new planar air-bearing microgravity simulator which has two distinctive features: separate air-bearings supporting each link of the manipulator and large area for the experiment. Experimental results are shown, in which end-effector is moving on a straight-line trajectory.

1. INTRODUCTION

There are many applications of autonomous robotic systems in space environment. Satellite equipped with a robotic-arm can be used for servicing commercial satellites (e.g., [1], [2], [3]) or capturing and removing space debris from orbit (e.g., [4], [5]). Control of a satellite-manipulator system is a challenging task, as interactions occur between the satellite and the robotic arm [6]. Such system lacks a fixed-base and it is difficult to test it on Earth due to gravitational conditions (in space, for free-floating system, motions of the manipulator affect satellite position and orientation). Certain technologies required for on-orbit satellite servicing were already verified during demonstration missions (e.g., ETS VII [7] or Orbital Express [8]) and new such missions are currently under development (e.g., DEOS [9], [10]). However, test-bed systems that would allow preliminary tests in Earth conditions are still indispensable. And, although certain limitations are inevitable, several solutions exist that take into account the dynamical aspects of a free-floating satellite-manipulator system (e.g., tests on parabolic flights [11]). The review of existing solutions was presented in [12].

Free two-dimensional motion of the satellite-manipulator system can be investigated experimentally on the planar-air bearing table. In such approach, satellite mock-up with attached robotic arm is mounted on air-bearings that allow almost frictionless motion on the table surface, thus simulating in two dimensions microgravity conditions and taking into account free-floating nature of the system. The use of planar air-bearing tables for space robotics has a long history [13]. Existing solutions differ in sizes and masses of system components, as well as number, type and location of air-bearings. Planar air-bearing microgravity simulators were used for the demonstration of control algorithms [14], to test specific components of docking mechanisms [15] and for tests preceding on-orbit demonstration missions [16]. It should also be noted that although systems that would allow three-dimensional tests on air-bearings were proposed (e.g., [17], [18]), they were not yet successfully constructed.

In this paper, we present a new planar air-bearing microgravity simulator constructed recently in the Space Research Centre of the Polish Academy of Sciences (early concept of this test-bed was presented in [19]). In section 2 this new test-bed is described in detail. Exemplary results of an experiment, in which end-effector is moving on a straight-line trajectory, are presented in section 3. Paper concludes with section 4.

2. AIR-BEARING TEST-BED

2.1. General description

The microgravity simulator constructed in the Space Research Centre PAS consists of a 2DoF manipulator mounted on a base (satellite mock-up). System can move and rotate freely on a plane, thus motions of the manipulator will affect position and orientation of the base. Area of the granite table, on which satellite-manipulator system can move, has dimensions of 2x3 meters and is larger than in many similar solutions (e.g., [20], [21]). The large size of this area allows tests of complex manoeuvres and gives possibility of future application of flexible manipulator links. Additional air-bearings are used to support independently each manipulator link, thus allowing tests of long and heavy manipulator (longer and heavier manipulator has more

significant influence on base position and orientation). The picture of aforedescribed test-bed is shown in the Fig. 1. Schematic view of the satellite-manipulator system is presented in the Fig. 2, while its key geometrical and mass properties are provided in the Tab. 1. The total length of the manipulator is 1.22 m, while mass of the entire system is 18.9 kg.

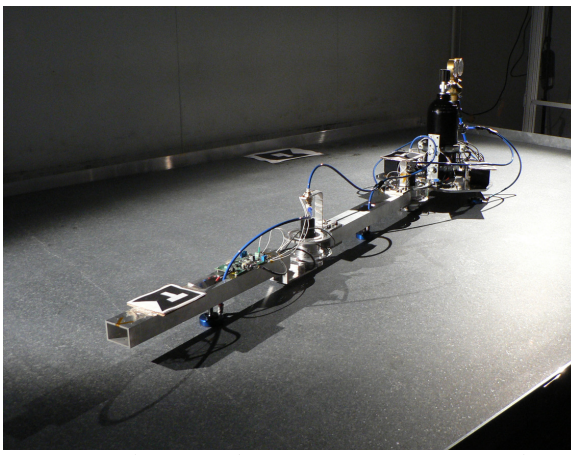

Figure 1. Planar air-bearing microgravity simulator

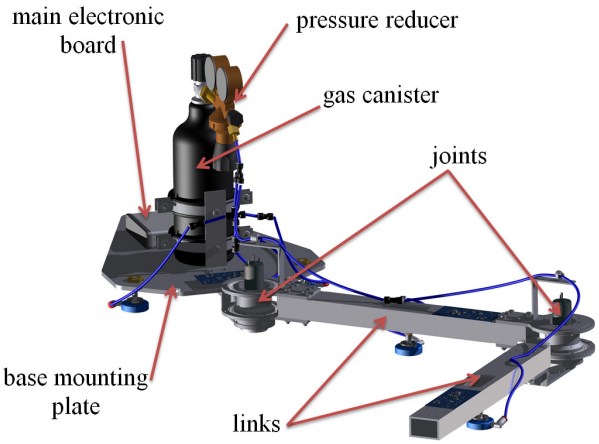

Figure 2. Schematic view of the planar satellite-manipulator system

Table 1. Geometrical and mass properties of the planar satellite-manipulator system

	Parameter	**Symbol**	**Value**
1	Base mass	m_0	12.9 kg
2	Base moment of inertia	I_0	0.208 kg·m^2
3	Link 1 mass	m_1	4.5 kg
4	Link 1 moment of inertia	I_1	0.32 kg·m^2
5	Link 1 length	l_1	0.62 m
6	Link 2 mass	m_2	1.5 kg
7	Link 2 moment of inertia	I_2	0.049 kg·m^2
8	Link 2 length	l_2	0.6 m
9	Mass ratio: $(m_1 + m_2)/ m_0$	k	0.465

2.2. Mechanical design

Both manipulator joints are rotational. Manipulator links are made from aluminium profiles, while moving base is an aluminium plate with gas canister attached in its centre. The main electronic board containing On Board Computer (OBC), joint-controller board (JC) for the first joint and batteries are also attached to the base, while joint-controller board for the second joint is attached to the first manipulator link. Pressurized air is distributed to all air bearings through flexible hoses. Rotational pneumatic connectors are used to transmit air through manipulator joints. Each joint consists of a DC motor, harmonic drive, two resilient suspension plates and absolute optical encoder. Picture of such joint is presented in the Fig. 3.

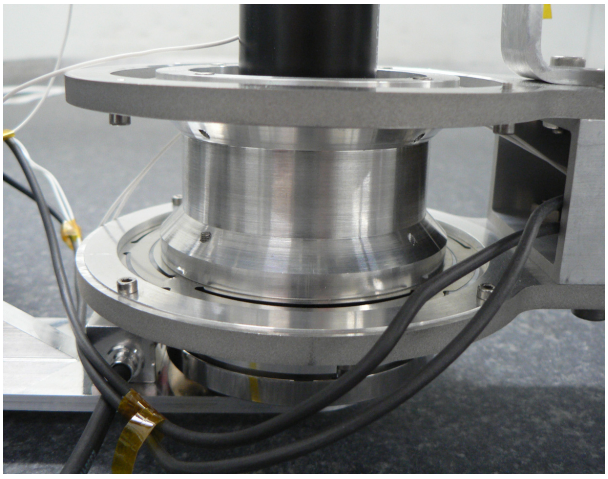

Figure 3. Picture of the manipulator joint

Three air bearings used to support the moving base form a three-point stance. This new test-bed was designed for investigations of systems with long links of the robotic arm and with significant mass of the robotic arm in comparison to the mass of the base. As a consequence, each link of the manipulator must be supported on its own air bearing. Adding these two air-bearings to three bearings supporting the base is a challenging task, as all five support points must be ideally coplanar in order to allow proper operation of the bearings and free planar motion of the system.

Each air bearing is mounted on a ball stud and resilient suspension plates are used in the manipulator joints for compensation of possible vertical misalignments between components of the system. These plates are made from spring steel and shaped in such a way that even modest forces acting in the vertical direction are sufficient to deform the plate and ensure vertical compensation of joints position, while at the same time plate is resistant to torques acting about the vertical axis.

2.3. Air-bearings

Air-bearings generate a thin film of pressurized air and slide on it. This film is 5 ÷ 15 μm thin – its thickness depends on the load carried by the air bearing. Air bearings based on a porous media technology are used in this test-bed (schematic view of such bearing is presented in the Fig. 4, while picture of actual bearing used in the test-bed is provided in the Fig. 5). Pressurized air is supplied through a hole on a side of the air-bearing and airflow is then controlled across the entire bearing surface through millions of holes in the porous carbon. Air pressure remains almost uniform across the whole surface, as the air flow is automatically restricted and damped. In contrast to classic air-bearings where the air is distributed through many small orifices, porous air bearings are immune to scratches and hard to clog. Protection ensured by the porous carbon results in no damage to bearing surface even in case of a sudden air supply failure.

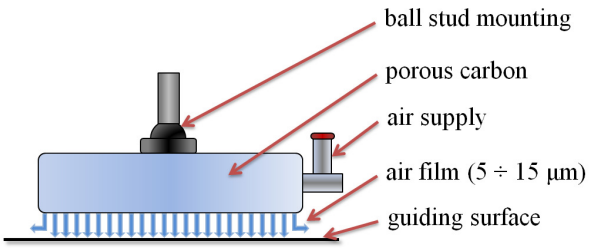

Figure 4. Schematic view of the air bearing

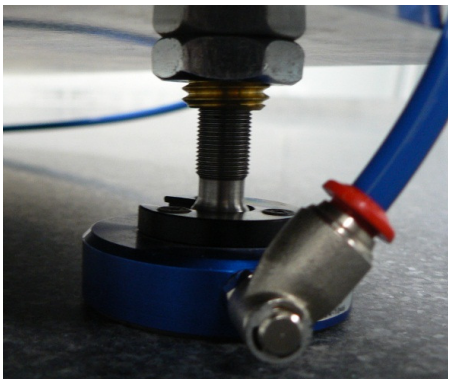

Figure 5. Air bearing used in the test-bed

2.4. Electronics and control system

The electronic subsystem used for the new planar air-bearing microgravity simulator consist of two kinds of electronic circuits: (i) On Board Computer (OBC) and (ii) two joint-controller boards (JC). Scheme of the entire control system is presented in the Fig. 6.

The OBC monitors, collects and stores all the data that comes from the executive subsystems (data logging up to 100 samples/s). It also performs mode management and trajectory planning. Control signals calculated by OBC are sent to the respective JC. Picture of OBC board is shown in the Fig. 7, while its main characteristics are presented in the Tab. 2. OBC bases on a 1GHz DM3730 Texas Instruments processor. The Flash and SD cards are used to store the application software and all the data collected during the test and measurement phase.

The multiple joint-controller board (JC) has the following tasks: to control the DC motor, to monitor the joints position through reading the encoder and to monitor its own electronics by collecting the data about the temperatures, supply current and voltage. The JC circuit consists of 32bits ARM Cortex M3 microcontroller, linear power converter, set of input/output buffers and RS-485 interface to communicate with the encoders. Logical blocks of JC are detailed in the Fig. 8.

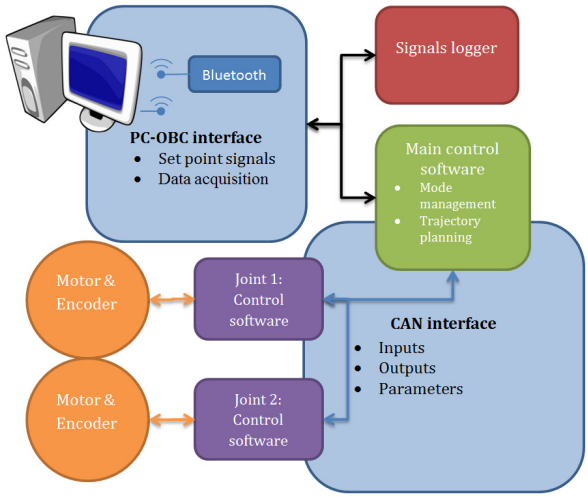

Figure 6. Scheme of the control system

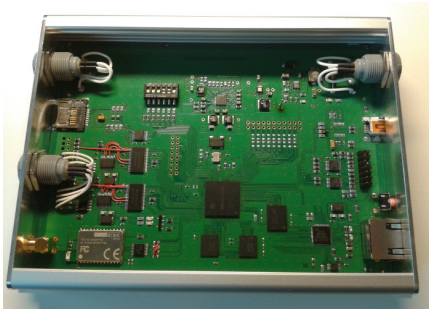

Figure 7. On Board Computer (OBC)

Table 2. The characteristics of the OBC

Parameter	Value
Mass	500 g
Supply voltage range	10 – 36 V
Power	2 W
Dimensions	184 x 125 x 34 mm
Mass memory	1 GB NAND Flash Max. 32 GB SD Flash

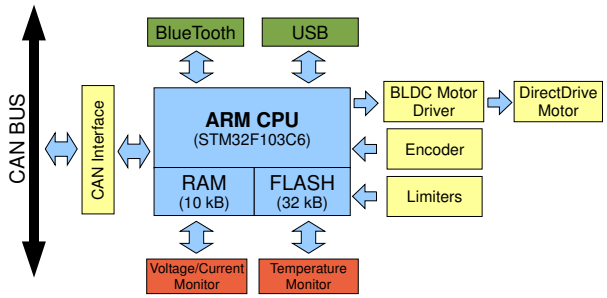

Figure 8. The logical blocks of JC

OBC and JCs are communicating with each other using CAN bus at 1Mbps. Special purpose CAN application level interface has been implemented on top of CAN bus to provide real time and robust transmission channel between systems nodes. During the manoeuvre it is responsible for transferring reference signals from trajectory planning block to specific joint control software and measured joint position from joint controllers to OBC. The whole embedded system uses Bluetooth interface to communicate with a host PC, on which human-machine interface application is running (OBC is equipped with Bluetooth unit that bases on WT12 from Bluegiga). Use of wireless communication is necessary, as any wires connecting the moving base with the external computer would affect free motion of the satellite-manipulator system.

2.5. Visual pose estimation

Visual pose estimation system is used to track the satellite-manipulator system during the experiment. Visual pose estimation provides position and orientation of both manipulator links and of manipulator base.

The visual markers used in the test-bed are designed in a way that makes them highly separable from background even at a large distance. Each marker is a black concave pentagon containing a square area in the middle which holds a pattern that makes the markers distinguishable between each other. We use pentagons, instead of classical squares [22], [23], because the extra point increases pose estimation accuracy and clearly defines the orientation of a marker without increasing the complexity of the detection process. To detect the markers, each incoming image is first thresholded to find all the dark blobs. For each blob, it is then necessary to find its outer contour and corners in order to discard the ones that are not pentagons. Subsequently lines are fitted to the points along each of the contours sides. The intersections of those lines provide corner locations with subpixel precision. Each blob area in the image is then warped to a standard shape in order to check if it contains a valid pattern.

Because the camera calibration parameters, marker position in the image and real marker shape are known, it is possible to estimate marker position relative to the camera. The pose is initially estimated from the homography between the marker and the camera plane. It is further optimized in an iterative process by minimizing the error between the reprojected marker position and its detected position in the image.

A frame from video recording captured by Nikon SLR digital camera is presented in the Fig. 9, on which detected markers were outlined by the pose estimation software.

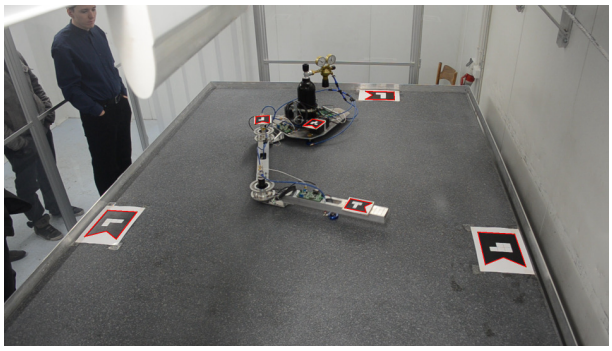

Figure 9. Frame captured by visual pose estimation system camera

3. EXPERIMENTAL RESULTS

Manipulator-equipped satellite must be considered as a free-floating object, unless it has precise attitude and position keeping system able to compensate for the motions of the manipulator. For control of a free-floating system, we follow General Jacobian Matrix (GJM) approach introduced in [24]. The system is described in the velocity space in order to determine driving torques for manipulator joint. For a given end-effector trajectory, velocities of manipulator joints are given by Eq. 1:

$$\dot{\mathbf{q}} = \left(\mathbf{J}_M - \mathbf{J}_S \mathbf{H}_2^{-1} \mathbf{H}_3 \right)^{-1} \begin{bmatrix} \mathbf{v}_{ee} \\ \boldsymbol{\omega}_{ee} \end{bmatrix}, \qquad (1)$$

where $\mathbf{v}_{ee}$ and $\boldsymbol{\omega}_{ee}$ are end-effector linear and angular velocities respectively, $\mathbf{J}_S$ and $\mathbf{J}_M$ are the Jacobians of the satellite and of the manipulator (for standard Earth manipulator). Matrices $\mathbf{H}_2$ and $\mathbf{H}_3$ (defined, e.g., in [25]) depend on the configuration of the manipulator and on the state of the satellite. During trajectory planning Eq. 1 is solved simultaneously with the equation for linear and angular velocity of the servicing satellite:

$$\begin{bmatrix} \mathbf{v}_S \\ \boldsymbol{\omega}_S \end{bmatrix} = -\mathbf{H}_2^{-1} \mathbf{H}_3 \dot{\mathbf{q}} \,. \qquad (2)$$

Eq. 1 and Eq. 2 are integrated by the numerical solver to obtain positions of manipulator joints and their derivatives. Subsequently, Eq. 3 can easily be used to compute driving torques Q for manipulator joints:

$$\mathbf{Q} = \mathbf{M}(\mathbf{q})\ddot{\mathbf{q}} + \mathbf{C}(\mathbf{q},\dot{\mathbf{q}})\dot{\mathbf{q}}, \qquad (3)$$

where **M** denotes generalized mass matrix and **C** denotes Coriolis matrix. Details of this approach are presented in [26]. In the experimental set-up, however, driving torques computed with Eq. 3 are not used, as joint controllers are only using reference joint positions for realization of a given trajectory.

In this paper, we present results of a simple experiment performed on the aforedescribed planar air-bearing microgravity simulator in order to verify its performance. Behaviour of the satellite-manipulator system observed on the air-bearing test-bed is compared with the results of the numerical simulations. The aim of this experiment was to achieve straight-line end-effector trajectory (in the inertial reference frame). In trajectory planning phase for a given reference end-effector trajectory Eq. 1 and Eq. 2 were used to compute reference trajectory in the configuration space (positions of manipulator joints). Joint controllers were responsible for realization of the trajectory and no feedback from end-effector position was used.

Reference positions of manipulator joints for straight-line end-effector trajectory are presented in the Fig. 10, while velocities of the joints are presented in the Fig. 11. Results of the demonstration performed on the planar air-bearing microgravity simulator are presented in the Fig. 12 – Fig. 14. Differences between the joints reference trajectory and data obtained from encoders is shown in the Fig. 12. These differences are very small during the entire manoeuvre. The comparison between the reference straight-line trajectory and the end-effector position obtained from the visual pose estimation system is presented in the Fig. 13. Total reference translation of the end-effector was 0.6 m (motion started at a point with inertial frame coordinates $x = 0.73$ m and $y = 2.1$ m). Motion of the manipulator induced the change of satellite orientation by nearly 112 degrees. Fig. 14 compares the satellite orientation obtained from the numerical simulations and orientation of manipulator base measured during the experiment.

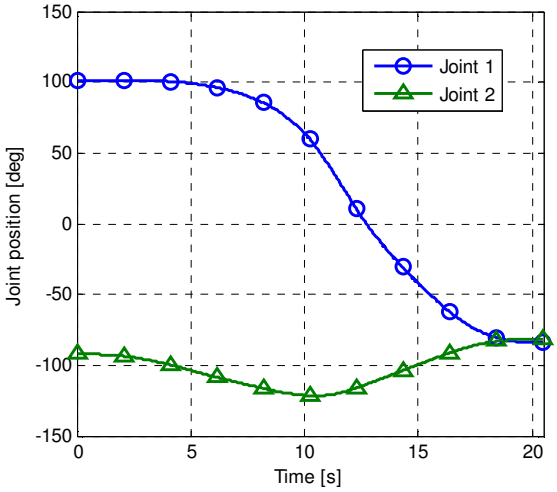

Figure 10. Positions of manipulator joints for straight-line trajectory (data used by the control system in the experiment)

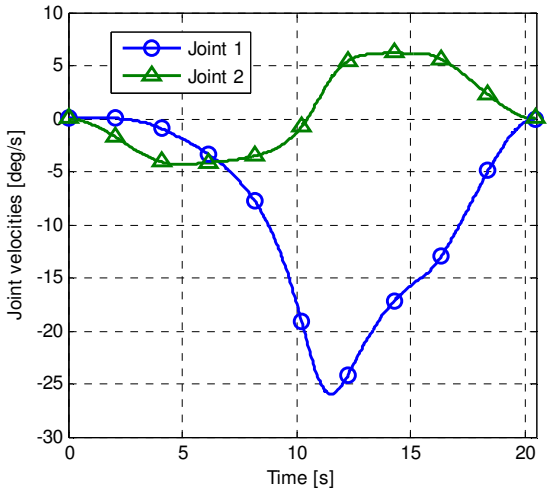

Figure 11. Velocities of manipulator joints for straight-line trajectory

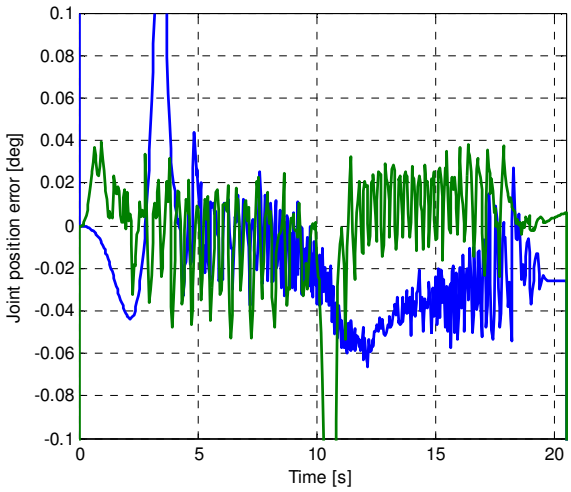

Figure 12. Error of position of manipulator joints during the experiment (difference between the given trajectory and data obtained from encoders)

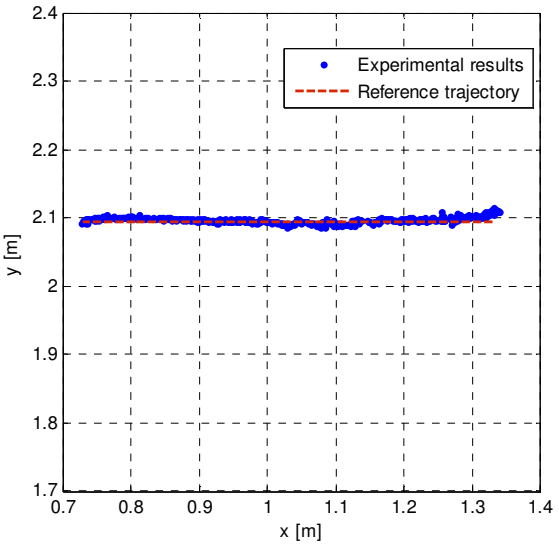

Figure 13. Comparison between the given end-effector straight-line trajectory and end-effector position measured during the experiment

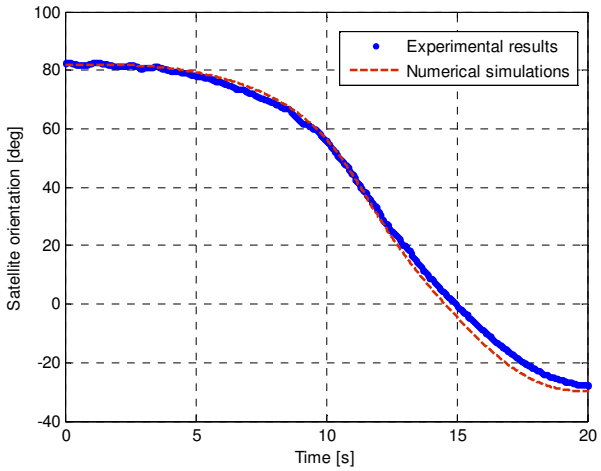

Figure 14. Comparison between the satellite orientation obtained from numerical simulations and orientation of manipulator base measured during the experiment

4. CONCLUSIONS

In this paper, the new planar air-bearing microgravity simulator constructed recently in the Space Research Centre of the Polish Academy of Sciences was presented. Although idea of such simulator is not new and test-beds based on the same principle of operations were described in various studies, this new simulator has two distinctive features: large area for the experiment (2x3 meters) and separate air-bearings supporting each link of the manipulator. Large area of the granite table surface is advantageous when one would like to perform complex manoeuvres of the satellite-manipulator system. It also allows addition of third link to the current 2DoF manipulator. Making manipulator redundant would extend the scope of control and trajectory planning methods that could be demonstrated on this microgravity simulator. The second important feature of the microgravity simulator described herein, i.e. air-bearing support for each manipulator link, gives the possibility to test systems with high ratio of the manipulator mass to the mass of the satellite. Control and trajectory planning for systems with higher value of this ratio is more difficult as the influence of the lack of fixed-base on the behaviour of such systems becomes more significant. Moreover, separate air-bearings under the links and the large area of the table makes it possible to test manipulator with long links, which is especially important when one wants to investigate links flexibility and control of systems with flexible links.

In the second part of this paper, exemplary experimental results were presented. In the performed experiment the end-effector was moving on a straight-line trajectory. GJM-based algorithm, sketched briefly in this paper, was applied to compute positions of the joints. In the performed test no feedback from the end-effector position was used (joint controllers were only responsible for trajectory following in manipulator configuration space). Nevertheless, end-effector trajectory obtained from the experiment is very close to the planned reference trajectory. Acquired measurements were compared with the results of numerical simulations and it was demonstrated that measured changes of the orientation of manipulator base show good agreement with these results. Of course, without the feedback from end-effector position, error in the realization of the trajectory in Cartesian coordinates is increasing, as any inaccuracies in the determination of the system mass and geometrical properties resulted in increasing error during integration of the equation used to calculate positions of the joints.

5. ACKNOWLEDGMENTS

This paper was partially supported by the National Centre for Research and Development project no. LIDER/10/89/L-2/10/NCBIR/2011.

6. REFERENCES

1. Yasaka, T. and Ashford, W. (1996). GSV: An Approach Toward Space System Servicing. *Earth Space Review* 5 (2), 9 – 17.

2. Visentin, G. and Brown, D.L. (1998). Robotics for Geostationary Satellite Servicing. *Robotics and Autonomous Systems* 23, 45 – 51,

3. Wenfu Xu, Bin Liang, Dai Gao, and Yangsheng Xu (2010). A Space Robotic System Used for On-Orbit Servicing in the Geostationary Orbit. In *Proc. 2010 IEEE/RSJ International Conference on Intelligent Robots and Systems*, Taipei, Taiwan.

4. Smith, D.A., Martin, C., Kassebom, M., Petersen, H., Shaw, A., Skidmore, B., Smith, D., Stokes, H. and Willig, A. (2004). A Mission to Preserve the Geostationary Region. *Advances in Space Research* 34, 1214 – 1218.

5. Rebele, B., Krenn, R. and Schäfer, B. (2002). Grasping Strategies and Dynamic Aspects in Satellite Capturing by Robotic Manipulator. In *Proc. 7th ESA Workshop on Advanced Space Technologies for Robotics and Automation 'ASTRA 2002'*, ESTEC, Noordwijk, The Netherlands.

6. Dubowsky, S. and Papadopoulos, E. (1993) The Kinematics, Dynamics and Control of Free-flying and Free-floating Space Robotic Systems. *IEEE Transactions on Robotics and Automation* 9 (5), 531 - 543.

7. Abiko, S. and Yoshida, K. (2001). Post Flight Analysis of ETS-VII Space Robotic Experiments. In *Proc. 6th International Symposium on Artificial Intelligence, Robotics and Automation in Space 'i-SAIRAS 2001'*, St-Hubert, Quebec, Canada.

8. Ogilvie, A., Allport, J., Hannah, M. and Lymer, J. (2008). Autonomous Satellite Servicing Using the Orbital Express Demonstration Manipulator System. In *Proc. 9th International Symposium on Artificial Intelligence, Robotics and Automation in Space 'i-SAIRAS',* Los Angeles, CA, USA.

9. Rupp, T., Boge, T., Kiehling, R. and Sellmaier, F. (2009). Flight Dynamics Challenges of the German On-Orbit Servicing Mission DEOS. In *Proc. 21st International Symposium on Space Flight Dynamics*, Toulouse, France.

10. Reintsema, D., Thaeterm J., Rathke, A., Naumann, W., Rank, P. and Sommer, J. (2010). DEOS – The German Robotics Approach to Secure and De-Orbit Malfunctioned Satellites from Low Earth Orbits. In *Proc. 10th International Symposium on Artificial Intelligence, Robotics and Automation in Space 'i-SAIRAS 2010',* Sapporo, Japan.

11. Menon, C., Aboudan, A.,Cocuzza, S., Bulgarelli, A. and Angrilli, F. (2005). Free-Flying Robot Tested on Parabolic Flights: Kinematic Control. *Journal of Guidance, Control, and Dynamics* 28(4), 623 - 630.

12. Menon, C., Busolo, S., Cocuzza, A., Aboudan, A., Bulgarelli, A., Bettanini, C., Marchesi, M. and Angrilli, F. (2007). Issues and solutions for testing free-flying robots. *Acta Astronautica* 60 (12), 957-965.

13. Schwarz, J., Peck, M. and Hall, C. (2003). Historical Review of Air-Bearing Spacecraft Simulators, *Journal of Guidance, Control and Dynamics* 26 (4), 513 - 522.

14. Marchesi, M., Angrilli, F. and Bettanini, C. (2001). On Ground Experiments of Free-flyer Space Robot Simulator in Intervention Missions. In *Proc. 6th International Symposium on Artificial Intelligence, Robotics and Automation in Space 'i-SAIRAS 2001'*, St-Hubert, Quebec, Canada.

15. Ma Ou, Yang, G., and Diao X. (2005) Experimental Validation of CDT-Based Satellite Docking Simulations Using SOSS Testbed. In *Proc. 8th International Symposium on Artificial Intelligence, Robotics and Automation in Space 'i-SAIRAS 2005'*, Munich, Germany.

16. Yoshida, K. (2003). Engineering Test Satellite VII Flight Experiments For Space Robot Dynamics and Control: Theories on Laboratory Test Beds Ten Years Ago, Now in Orbit. *The International Journal of Robotics Research* 22 (5), 321 – 335.

17. Okamoto, O., Nakayat, T. and Pokinestt, B. (1994). Concept Verification of Three Dimensional Free Motion Simulator for Space Robot In *Proc. 3rd International Symposium on Artificial Intelligence, Robotics and Automation in Space 'i-SAIRAS 1994'*, Pasadena, California, USA,

18. Viswanathan S.P., Sanyal, A. and Holguin, L. (2012) Dynamics and Control of a Six Degrees of Freedom Ground Simulator for Autonomous Rendezvous and Proximity Operation of Spacecraft. In *Proc. AIAA Guidance, Navigation, and Control Conference 2012*, Minneapolis, USA.

19. Rybus, T., Seweryn, K., Banaszkiewicz, M., Macioszek, K., Maediger, B. and Sommer, J. (2012). Dynamic simulations of free-floating space robots. In *Robot Motion and Control 2011, Lecture Notes in Control and Information Sciences* 422, Ed. Krzysztof. R. Kozłowski, Springer-Verlag, 351 - 361.

20. Yoshida, K. and Umetani, Y. (1990). Control of Space Free-Flying Robot. In *Proc. 29th IEEE Conference on Decision and Control*, Honolulu, Hawaii, 97 - 102.

21. Papadopoulos, E., Paraskevas, I.S., Flessa, T., Nanos, K., Rekleitis, G. and Kontolatis, I. (2008). The NTUA Space Robot Simulator: Design & Results. In *Proc. 10th ESA Workshop on Advanced Space Technologies for Robotics and Automation 'ASTRA 2008'*, ESTEC, Noordwijk, The Netherlands.

22. Kato, H. and Billinghurst, M. (1999). Marker Tracking and HMD Calibration for a video-based Augmented Reality Conferencing System. In *Proc. 2nd International Workshop on Augmented Reality 'IWAR 99'*, USA, 85 - 94.

23. Fiala, M. (2004). ARTag, An Improved Marker System Based on ARToolkit. National Research Council Canada, Publication Number: NRC 47166.

24. Umetani, Y. and Yoshida, K. (1989). Resolved Motion Rate Control of Space Manipulators with Generalized Jacobian Matrix. *IEEE Transactions on Robotics and Automation* 5 (3), 303 - 314.

25. Seweryn, K. and Banaszkiewicz, M. (2008). Optimization of the trajectory of an general free – flying manipulator during the rendezvous maneuver. In *Proc. AIAA Guidance, Navigation and Control Conference and Exhibit 2008*, Honolulu, Hawaii, USA.

26. Rybus, T. and Seweryn, K. (2013). Trajectory planning and simulations of the manipulator mounted on a free-floating satellite. In *Aerospace Robotics, GeoPlanet: Earth and Planetary Sciences*, Ed. Jurek Z. Sasiadek, Springer-Verlag, 2013.